HHS Public Access

Author manuscript

Magn Reson Imaging. Author manuscript; available in PMC 2020 April 20.

Published in final edited form as:

Magn Reson Imaging. 2019 October ; 62: 94–103. doi:10.1016/j.mri.2019.06.020.

Can post-chemotherapy cardiotoxicity be detected in long-term survivors of breast cancer via comprehensive 3D left-ventricular contractility (strain) analysis?

Julia Kar[a,*], **Michael V. Cohen**[b], **Samuel A. McQuiston**[c], **Maria S. Figarola**[c], **Christopher M. Malozzi**[b]

[a]Departments of Mechanical Engineering and Pharmacology, University of South Alabama, 150 Jaguar Drive, Mobile, AL 36688, United States of America

[b]Department of Cardiology, College of Medicine, University of South Alabama, 1700 Center Street, Mobile, AL 36604, United States of America

[c]Department of Radiology, University of South Alabama, 2451 USA Medical Center Drive, Mobile, AL 36617, United States of America

Abstract

Purpose: This study applied a novel and automated contractility analysis tool to investigate possible cardiotoxicity-related left-ventricular (LV) dysfunction in breast cancer patients following treatment with anti-neoplastic chemotherapy agents (CTA). Subclinical dysfunction otherwise undetected via LV ejection fraction (LVEF) was determined.

Methods: Deformation data were acquired with the Displacement Encoding with Stimulated Echoes (DENSE) MRI sequence on 16 female patients who had CTA-based treatment. The contractility analysis tool consisting of image quantization-based boundary detection and the meshfree Radial Point Interpolation Method was used to compare chamber quantifications, 3D regional strains and torsion between patients and healthy subjects (N = 26 females with N = 14 age-matched). Quantifications of patient LVEFs from DENSE and Steady-State Free Precession (SSFP) acquisitions were compared, Bland-Altman interobserver agreements measured on their strain results and differences in contractile parameters with healthy subjects determined via Student's *t*-tests.

Results: A significant difference was not found between DENSE and SSFP-based patient LVEFs at 58 ± 7% vs 57 ± 9%, p = 0.6. Bland-Altman agreements were − 0.01 ± 0.05 for longitudinal strain and 0.1 ± 1.3° for torsion. Differences in basal diameter indicating enlargement, 5.2 ± 0.5 cm vs 4.5 ± 0.5 cm, p < 0.01, and torsion, 4.7 ± 1.0° vs 8.1 ± 1.1°, p < 0.001 in the mid-ventricle

[*]Corresponding author. jkar@southalabama.edu (J. Kar).

Declaration of Competing Interests

As authors we confirm that none of us have any competing interests in the manuscript. Hence, there are no potential conflict of interests with any entities within the University of South Alabama or outside including institutes, organizations and commercial entities.

Availability of data

Data related to this project can be obtained from the Open Science Framework repository at URL: https://osf.io/76y8t/ DOI: 10.17605/OSF.IO/76Y8T or upon request to the corresponding author, Julia Kar, PhD, jkar@southalabama.edu

and 5.9 ± 1.2° vs 10.2 ± 0.9°, $p < 0.001$ apically, were seen between patients and age-matched healthy subjects and similarly in longitudinal strain, but not in LVEF.

Conclusions: Results from the statistical analysis reveal the likelihood of LV remodeling in this patient subpopulation otherwise not indicated by LVEF measurements.

Keywords

Cardiotoxicity; Breast Cancer; DENSE; RPIM; Left-ventricular contractility; 3D strain; LVEF

1. Introduction

The administration of certain anti-neoplastic chemotherapeutic agents (CTA), such as anthracyclines and trastuzumab, in breast cancer patients may lead to the complications of developing cardiotoxicity, and counter any gains in survivorship achieved with this form of treatment [1–6]. The cardiotoxicity-based dysfunctions caused by CTAs that range from arrhythmias to irreversible heart failure require robust and managed care, such as guideline directed medical therapy (GDMT) that ensure patient longevity [7]. Hence, chemotherapy treatment plans that incorporate CTA doses should include cardiotoxicity surveillance consisting of routine monitoring of left-ventricular (LV) contractility such that the onset of irreversible damage and heart failure incidences can be prevented [1,3,8–15]. To this effect, scientific evidence and a growing number of clinical studies now show that a most effective way of monitoring contractile pattern changes is via computations of LV myocardial strain, which is a metric of contractile function now proven to be a more sensitive biomarker for detecting cardiotoxicity than dysfunction measured via reductions in LV ejection fraction (LVEF) [9,13,16–20].

1.1. The epidemiology of cardiotoxicity and importance of subclinical contractility measurements

In its highly recurrent manifestation, CTA-induced cardiotoxicity continue to cause progressive LV dysfunction that manifest as (hypo-kinetic) dilated cardiomyopathy (DCM) and symptomatic heart failure in breast cancer [1,2,5,15,21]. It is well established that the management of cardiotoxicity is invariably complicated and the response to medical therapy generally poor when heart failure manifests due to CTA mediated cardiotoxicity [5,9,13,22]. Hence, subclinical detections of cardiotoxicity that may incorporate modifications of dose, administration rates of CTAs, or enable interventions with cardiac drugs such as enalapril or carvedilol is highly recommended [1,8]. However, the standard accepted measure of cardiotoxicity, defined as a decline in echocardiographic quantification of LVEF, may not always provide optimal information regarding subclinical detection [2,7]. There is confusion regarding what LVEF decrements qualify as clinically significant, which limits monitoring of subclinical cardiac damage until a later stage when meaningful clinical management becomes ineffective. In regards to different surveillance mechanisms, preclinical studies now show that image-based measurements of LV myocardial strain can provide early and sensitive detection of subclinical cardiotoxicity prior to reductions in LVEF either during or shortly following chemotherapy regimens [5,10,13,17,18]. For example, in breast cancer studies of patients treated with anthracyclines like doxorubicin, trastuzumab and taxol there

was no significant changes in LVEF but longitudinal and radial strains and strain rate changes were observed [13,16]. Studies in functional twist and torsion based myocardial deterioration have also shown preserved LVEF as being non-indicative of altered LV mechanics [9,11,12]. As an overall summary, > 15 peer-reviewed studies to date now show decreased strain, strain-rates, twist and torsion where almost half these studies do not show changed LVEF [23].

Hence, this study was motivated by the need to investigate if subclinical cardiac remodeling that may occur in post-chemotherapy patients, which remain undetected by a reduced LVEF, can be detected via differences in LV chamber quantifications and 3D strain computations in comparison to healthy subjects.

2. Materials and methods

2.1. Scope of study

This study investigated the feasibility of a fully automated, single-scan, MRI-based methodology for LV chamber quantifications and 3D strain computations toward detecting any cardiac remodeling that may occur in survivors of breast cancer who have undergone CTA-based chemotherapy [33]. Of particular note was targeted computations of LV torsion (in addition to 3D strains) given a prevailing emphasis in the scientific community that any abnormal torsion indicates the altered wringing motions in the heart's myofibers during ejection, thus making it a major indicator of cardiac dysfunction [25–27]. The detection algorithm consists of a novel and automated 3D methodology that rapidly tracks LV boundary motion and analyzes 3D strains following phase-unwrapping of MRI data obtained with the navigator-gated, spiral Displacement Encoding with Stimulated Echoes (DENSE) sequence [28–33]. Following analysis, this technique is capable of generating 3D surface maps in all six independent strain directions as well as torsion. As an additional validation step for the automated algorithm's boundary detection and reconstruction technique, comparisons were made between patient LVEFs computed from DENSE and corresponding Steady State Free Precession (SSFP) images, and in addition, between the DENSE and their transthoracic echocardiogram (TTE) exam LVEFs. All contractile measurements, inclusive of chamber quantifications, 3D strains and torsion, in the patient subpopulation were then compared to our database of healthy subjects (N = 26 females).

2.2. Human subject recruitments

The possibility of cardiac remodeling and occurrence of LV dysfunction was tested on DENSE data acquired in 16 adult breast cancer survivors. The patients had undergone CTA-based (anthracyclines and trastuzumab) chemotherapy and were under continued surveillance and some under a regimen of managed care for non-acute cardiac complications related to cardiotoxicity (such as stage I hypertension or diabetes mellitus rated at NYHA class ≤ II). In general, to rule out the effects of acute cardiac comorbidities influencing their strain data, the exclusion criteria for these patients included LVEF < 50%, valvular heart disease, ischemic heart disease and acute infarction, severe hypertension and a terminal life of expectancy < 3 months. The most important criteria for recruitment were the absence of acute cardiac complications and a preserved LVEF > 50% at the inception of chemotherapy

as measured with TTE. Due to the likelihood of developing common cardiac side-effects following chemotherapy, patients were not excluded if they had developed non-acute conditions that often follow CTA-based chemotherapy, such as non-severe arrhythmias (absence of atrial or ventricular fibrillation), hypertension (stage I) or < 10% drop in LVEF but preserved at LVEF > 50% [1,34]. Hence, patients who had cardiac comorbidities rated above a NYHA class II were not included. Radiation therapy is an integral component of the management of breast cancer that effectively reduce local recurrences and like other studies patients who underwent radiation therapy were not excluded [9,15,16]. Furthermore, as we state next, the timing of patient recruitment (within 12 months of chemotherapy treatment) is too early for the manifestation of radiotherapy effects where the estimated aggregate incidence of cardiac disease due to radiation is 5–10 years post-treatment [35]. Hence, the timeline for recruiting patients was within 12 months from the end of their chemotherapy as the most frequent and clinically relevant form of cardiotoxicity occurs within this period [10,15]. The MRI study in each patient was scheduled after a post-chemotherapy TTE exam to ensure their DENSE and TTE-based LVEF were comparable. Hence, they were consecutively recruited within the timeframe of this study with MRI acquisitions following their TTE and given they met the above cardiac risk criteria. For their treatment, the patients in this study had undergone either one of the following chemotherapy regimens (with individual patient-based modifications), including 1. ACT (60 mg/m^2 of doxorubicin and cyclophosphamide, 4 cycles, and taxol, for 4 cycles or weekly for 12 weeks), 2. TCH(P) (8 mg/kg loading + 6 mg/kg trastuzumab, taxol, carboplatin and with/without pertuzumab for 6 cycles, followed by 6 mg/kg trastuzumab with/without 8 mg/kg initial loading for a year). Additional full LV short-axis data with SSFP were acquired in the patients in order to validate their LVEF measurements. The patients were imaged in a 1.5 Tesla Espree (Siemens, Erlangen, Germany) MRI scanner using the navigator-gated 3D Spiral DENSE sequence [31,32]. All patients signed informed consents in accordance with the university's Institutional Review Board (IRB) guidelines and who volunteered access to their breast cancer and cardiac treatment plans for the purposes of this retrospective study. The healthy subjects are from a database of 48 (females and males) of whom N = 26 are females and N = 14 females age-matched to the patients with their data acquired using the same navigator-gated DENSE MRI sequence over the span of several of our validation studies. It is noted that healthy subjects were pre-evaluated on existing cardiac conditions and exempted from the study if they had such comorbidities. As all chemotherapy patients were females, comparisons of contractile parameters were made to the healthy age-matched female subset (N = 14) or the entire healthy female subgroup (N = 26) and the term healthy subjects henceforth imply females only.

2.3. DENSE acquisition and protocols

Navigator-gated, spiral 3D DENSE data were acquired with displacement encoding applied in two orthogonal in-plane directions and one through-plane direction [28,29,32,36]. An anterior 18-channel flexible array coil in combination with 12–16 elements of the table-mounted spine array coil were used for receiving signals on a 1.5 T scanner MAGNETOM Espree (Siemens Healthcare, Erlangen, Germany) [37]. Typical imaging parameters included field of view (FOV) of 380 × 380 mm, echo time (TE) of 1.04 ms, repetition time (TR) of 15 ms, flip angle (FA) of 20°, matrix size of 128 × 128 × 19, 2.97 × 2.97 × 5 mm voxel size, 21

cardiac phases, encoding frequency of 0.06 cycles/mm, simple 4-point encoding and 3-point phase cycling for artifact suppression [31,32]. The SSFP acquisition consisted of a FOV of 340 × 276 mm, TE of 1.48 ms, TR of 51.15 ms, FA of 80°, matrix size of 192 × 156 × 12, 1.77 × 1.77 mm pixel size, slice thickness of 7 mm and 25 cardiac phases. Heart rates (HR) and diastolic and systolic blood pressure s (DBP, SBP) were continuously monitored using a NT3C (Solaris Medical Technologies Inc., San Francisco, CA) monitor during the scans.

2.4. Automated boundary detection

As outlined in our previous publication this automated process consists of identifying the left-ventricular boundary contours in the most basal short-axis slice at end-diastole with the operator selecting an ellipsoidal region of interest (ROI), and followed by propagating the boundaries to all short axis slice positions between end-diastole and end-systole, as well as base to apex [33]. The LV boundaries and intramural tissue are identified using Otsu's Method which is a non-uniform quantization-based on image histogram bins that yields a threshold-based image with a distinct profile of the short-axis [38,39]. Additionally, this study is unique in combining the unwrapped displacement vectors toward precisely tracking and re-locating a boundary point between end-diastole and end-systole [28,29,32,40,41]. Following the generation of boundaries for all partitions and timeframes using the above technique as well as reconstructing the 3D LV, chamber quantifications included measuring diastolic and systolic chamber diameters, end-diastolic volume (EDV), end-systolic volume (ESV), stroke volume (SV), LVEF and LV mass (LVM) [33].

2.5. Meshfree strain analysis

Three-dimensional strain tensors were computed using the radial point interpolation method (RPIM) at each voxel in the patient's reconstructed 3D geometries. RPIM is a numerical analysis technique based on the Galerkin weak form that uses radial basis functions (RBF) as shape functions, which facilitates fast multidimensional computations of strain. Extensive descriptions of computing 3D LV strains with RPIM and by using Multiquadrics (MQ) as RBF shape function are outlined in our previous literature [36,40,42–44]. The LV torsion definition used in this study was the relative angle of twist between basal and apical rotations, and given by [25],

$$\alpha_T = \frac{(\varphi_{base} - \varphi_{apex})(\rho_{base} + \rho_{apex})}{2D} \quad (1)$$

where φ is the angle of twist, ρ is the radius, and D is the inter-segment distance. Using the above methodologies for boundary detection and strain analysis, contractile parameters in patients and healthy subjects were computed to observe if strains, torsion and chamber dimensions differed significantly.

2.6. Statistical analysis

For purposes of validation, the results of patient LVEFs computed using the automated algorithm from their DENSE magnitude images and SSFP (same day acquisitions) were compared via paired *t*-tests, and also between DENSE and their TTE LVEFs following chemotherapy. The methodology for analyzing strain in this study is a validated and

established research protocol that has been used in previous studies involving both patients and healthy subjects. Using the above technique, measurements of patient strains were conducted by two independent users (a radiology researcher and a graduate engineer) and interobserver agreements established with Bland-Altman analysis. Homoscedastic two-sample *t*-tests were used to compare all contractile parameters between patients and healthy subjects and LV remodeling and dysfunction in patients observed via significant differences ($p < 0.05$). As there was a age difference between the healthy subjects and patient subpopulation and given that recent population studies emphasize age and gender specific normal ranges for clinical use, age-specific comparisons of the parameters were conducted using a subset (N = 14) of the healthy subjects whose mean age was closest in comparison to the patient subpopulation [45–47]. A brief summary of comparisons to the entire healthy subgroup (N = 26) is also provided later in the results. Statistics related to demographics, strain and chamber parameters targeted for computations in all groups were for age, body mass, body mass index (BMI), body surface areas (BSA), DBP, SBP, HR, radial, circumferential and longitudinal strains, rotations and torsions, LV diameters, EDV, ESV, SV, LVEF and LVM.

3. Results

Detailed information regarding demographics, existing comorbidities and chamber quantifications are given in Table 1 for both patients and the age-matched healthy subjects (no comorbidities). The chemotherapy regimens the patients were under included 11/16 under ACT and 5/16 under TCH(P). In regards to radiotherapy and existing co-morbidities, six patients (4/16 left-sided) had undergone radiotherapy, two patients had diabetes mellitus (fasting blood sugar > 125 mg/dL), three had hypercholesterolemia (LDL > 190 mg/dL) and four had hypertension (SBP/DBP > 140/90 mmHg). The recruitment time for the patients was 5.5 ± 4 months from the end of their treatment and their MRI scan scheduled within a 1–3 days window of a post-chemotherapy TTE. Strain and torsional contractile parameters in these two subgroups are given in Table 2.

Results from comparing post-chemotherapy DENSE-based patient LVEFs vs their latest TTE results were 58 ± 7% vs 57 ± 8% ($p = 0.5$). Similar results from comparisons of LVEF measured with DENSE and SSFP were 58 ± 7% vs 57 ± 9% ($p = 0.6$) for the full LV. The patients' mean pre-chemotherapy TTE-based LVEF was 61 ± 7% which was not found to be significantly different from the LVEF of 62 ± 5% ($p = 0.8$) in healthy subjects. Fig. 1 shows slices of similar dimensions at the base-to-mid junction location from the two imaging protocols. Fig. 2 shows representative 3D displacement vectors in one patient and one healthy subject. The trend in Fig. 2 show the general disarrangement of displacement vectors that is typical to this patient subpopulation, with the abnormal leftward displacements being characteristic to the occurrence of DCM that is a common side-effect of early onset cardiotoxicity [1,11,22]. Additionally, Fig. 2 shows the trend toward LV enlargement, which is evident from the significantly different larger basal diameter in patients given in Table 1. The interobserver Bland-Altman agreements related to computations of normal strains and torsion in cardiotoxicity patients are shown in Fig. 3 where low biases and limits of agreement (−0.01 ± 0.06 for radial strain, 0.01 ± 0.03 for circumferential strain, −0.01 ± 0.05 for longitudinal strain and 0.1 ± 1.3° for torsion) can be seen. Fig. 4 extensively

represents the contractile parameters that were targeted for this study and shows the strain-time curves of basal, mid-ventricular and apical strains, mid-ventricular and apical torsion and full LVEF in both patients and healthy subjects. Visually it is seen that peak longitudinal strains and torsion are significantly different from healthy subjects as also given in Table 2. Furthermore, Table 2 shows the significantly different rotations between groups with it being a fundamental parameter toward computing torsion. In contrast, the peak radial and circumferential strains and LVEF are not different as also given by the significant differences in Tables 1 and 2. Fig. 5 show 3D surface strain maps in the entire LV for circumferential and longitudinal strains and torsion in a representative patient and healthy subject. The 3D plots show a generally enlarged LV in the particular patient (representative of this subpopulation as in Fig. 2) and the reduction in magnitudes of longitudinal strain and torsion but only slight differences in circumferential strain.

3.1. Comparisons to entire healthy subgroup

In the entire healthy subgroup, the mean age was 42.1 ± 10.9 years with $p < 0.01$ when compared to the patient subpopulation, body mass was 72.5 ± 16.4 kg ($p = 0.4$), BMI was 27.0 ± 5.1 kg/m^2 ($p = 0.5$) BSA was 1.8 ± 0.3 m^2 ($p = 0.4$), monitored mean HR was 70.4 ± 7.0 bpm ($p = 0.06$) and mean BP was 121.2 ± 8.3/69.8 ± 6.6 mmHg ($p = 0.3$, $p = 0.2$). Similarly, the results of global strains in the entire healthy subgroup were 0.33 ± 0.06 ($p = 0.3$) for radial, −0.22 ± 0.03 ($p = 0.08$) for circumferential and − 0.21 ± 0.03 ($p < 0.001$) for longitudinal strains and 7.3 ± 1.2° ($p < 0.001$) in the mid-ventricular and 9.0 ± 1.3° ($p < 0.001$) in apical torsion. Hence, significant differences were found between the patients and entire healthy subgroup in longitudinal strains and torsion. Basal diastolic diameter was 4.4 ± 0.5 cm ($p < 0.001$) which was significantly different but not LVEF, 63 ± 5% ($p = 0.05$) or LVM, 129.3 ± 8.3 g ($p = 0.4$). The above data show that differences in contractile parameters between patients and the entire healthy subgroup were very similar to the differences found between patients and the age-matched subset. Fig. 4 shows the systolic trajectories of parameters in the entire healthy subgroup compared to patients and the age-matched subset.

4. Discussion

This paper presents the findings of cardiotoxicity investigated in a population of breast cancer patients who underwent CTA-based chemotherapy with a validated and automated methodology used for determining LV contractile parameters. Systolic contractile parameters of the LV were computed with multi-threshold based quantization of DENSE magnitude images and meshfree RPIM strain analysis. Fig. 1 is representative of the additional validation step taken in comparing DENSE and SSFP-based LVEFs, with similarities in results proving the accuracy of the automated quantization-based technique. Fig. 2 shows the outcome of the initial step in computing deformation parameters (with phase-unwrapping) that lead to boundary detections, 3D LV re-constructions and strain computations. It is shown in Fig. 3 that the biases in the contractile parameters computed in the patient subpopulation are negligible and the limits of agreement range no higher than ~0.06 in non-dimensional strain magnitude for the radial, circumferential and longitudinal strains and < 1.5° in torsional agreement. Thus, these agreements can be considered strong background validation for the subclinical myocardial abnormalities that were (not) indicated

by the above parameters. Finally, most important to this study was determining the LV contractile parameters that significantly differed between CTA treated patients and age-matched healthy subjects, which were found to be in longitudinal strains, torsion and the basal diameter-based distortion as detailed in Tables 1–2 and visually seen in Figs. 4–5. The above summarize the key findings in the study, particularly when significant differences were not seen in LVEF (also circumferential and radial strains) between patients and healthy subjects.

The results in this study had good consistency with previous studies in literature [11,16,21]. The fact that under administration of CTA doses LV remodeling cause imminent cardiac dysfunction was shown in a study by Siedman et al., which found systolic abnormalities when patients were administered similar combined (or either) doses of anthracyclines and trastuzumab as in this study [21]. Studies also show that myocardial dysfunction related to subclinical cardiotoxicity can be detected earlier with altered global and regional 3D strains than with significant reductions in LVEF [2,11,13,16,18,23,48]. It is shown in our recent case-study where cardiotoxicity was first indicated by lower torsion and longitudinal strain in a 54 year old female chemotherapy patient treated with Adriamycin, cyclophosphamide and Herceptin and who later received Ado–Trastuzumab Emtansine but her LVEF was at 48% [49]. Following the strain-based findings, a TTE reexamination after two-months showed a drop in LVEF to < 25% which meant > 10% drop between subsequent tests that conform to GDMT-based diagnosis of cardiotoxicity in breast cancer patients. Her case is excluded from this study due to the existence of acute cardiac complications and her very low ejection fraction. Other studies show reduced peak systolic longitudinal strain between 9 and 19% and torsional reductions as high as 50% and this effect is seen in this study with the reduced peak longitudinal strains and torsion, which is not seen via LVEF reductions (Table 2 and Fig. 4) [11,23]. Very similar to our study, the ability to detect impaired functionality (cardiotoxicity) in the LV with strain parameters were shown previously by two others, one study by Sawaya et al. showed a decline in longitudinal strain following treatment with anthracyclines, trastuzumab and taxanes and the other by Motoki et al. showed declined torsion in patients treated with anthracyclines [11,16]. After showing a significant negative correlation between cumulative anthracycline dose and torsion, Motoki et al. emphasized that such torsional deformation was obvious due to cardiotoxicity affecting the helical orientation of myofibers. A number of studies in other LV impairments have also shown altered patterns in torsion due to adverse effects on fiber orientation, for example the divergent rotation patterns in the same direction at all levels that are found in DCM [25]. While not a fully divergent pattern, a significantly reduced basal rotation is seen in the patient subpopulation which could possibly arise from cardio-myocyte damage that eventually leads to the development of DCM, the most prevalent form of cardiac dysfunction that arise from CTA treatment [1,11,22]. The possibility of DCM occurrence is further enhanced by the septal bias and general disarrangement in the displacement patterns (represented in Fig. 2) which was seen in several patients. The above dysfunctional pattern was also reported in our previous studies as being distinctly characteristic to DCM [36,50]. Similarities not found with existing studies include not finding a reduction in peak systolic radial strain that have been reported as high as 40% or in peak systolic circumferential strain between 11 and 17% [9–12,16,17]. Another dissimilarity was an enlarged basal LV chamber

diameter of ~5.2 cm, which is in contrast to that found by the Motoki et al. study estimated at ~4.4 cm and possibly a later effect of DCM where the Motoki et al. study did not continue after 3 months [11].

It was also shown that similar significant differences in basal diameter, longitudinal strain and torsion exist between the patients and the entire healthy subgroup as with the age-matched subset. The similarities between the two comparisons are attributed to the moderate changes in contractile parameters that occur in healthy subjects in their mid-adult ages, in comparison to very significant changes that occur between adolescence and early adulthood or with later-age transition to elderly, as shown by recent studies [45–47]. For example, studies show that in females longitudinal strain changes are ~0.00–0.04 globally and regionally for an age range of 37.7 to 70 years and LVEF varies by ~0–2% in a similar age range [45,47]. Yet another suggested single measurements for radial and longitudinal strains in a healthy subgroup aged 41–59 years for reference use in clinical diagnosis [47,51]. The findings in this study are comparable to the above with longitudinal strains differing by ~0.02 and LVEF differences of ~1% between the age-matched subset and full healthy subgroup (Fig. 4). Among parameters that do change significantly over all ages is torsion which studies show substantially changing with each decade by 0.14°/cm, defined as the twist between apex and base per unit height of the LV [46]. This effect was seen in the ~1.5–2° non-normalized (to ventricular height) difference in torsion found between the age-matched subset and entire healthy subgroup. Overall, it is important to note that detection of subclinical contractile abnormalities was based on comparing two different subpopulations, patients and healthy subjects, which was possible due to the chamber quantifications and normal strain measurements in the database of healthy subjects we have built over several validation studies [33,50,52,53].

The first limitation of this study is that it is not a longitudinal study where the extent of remodeling in the patient LVs is tracked with time. However, this study has been important in confirming the presence of significant differences in contractile parameters, which provides a precedence for future studies that will target following incremental time-based changes after chemotherapy. A second limitation is the difference in age between the patient (~54.9 years) and the entire reference healthy subgroup (~42.1 years). However, recent studies show that for healthy subjects small insignificant changes occur for a number of the contractile parameters in the above age range [45–47,51]. Also, while we have shown that similar differences in contractile parameters exist when we compare patient parameters to either the entire healthy subgroup or an age-matched subset, further knowledge regarding contractile differences will be gained as we continue studying more patients. The third limitation lies in not comparing the automated boundaries to boundaries manually contoured by observers (generally an extremely tedious undertaking for the full LV) toward verifying the automated LVEF computations. A final limitation is not adjusting patient strains according to existing comorbidities via comparison to a pre-chemotherapy MRI scan. However, their strain parameters were assumed to be in the healthy range at the reference pre-chemotherapy time point with TTE-based LVEF > 50% and the absence of acute cardiac comorbidities. This limitation also includes the influence of radiotherapy, which may cause LV fibrosis and modify the development of cardiotoxicity. However, recent studies show that negligible differences existed between irradiated and non-irradiated patients with modern

therapeutic approaches and neither a cumulative anthracycline dose > 450 mg/m^2 nor a cardiac risk of NYHA class > III apply to this study [15,35].

5. Conclusion

This study shows that cardiac remodeling following treatment with chemotherapeutic agents such anthracycline and trastuzumab can be detected with the validated procedure for fast, inexpensive and automated strain analysis and mapping that is presented. The findings emphasize that basal LV diameters, longitudinal strains and torsion are metrics capable of detecting the altered LV function and remodeling otherwise not indicated by LVEF. However, the thresholds for these metrics will require rigorous clinical evaluations before they can be considered as diagnostic parameters that define myocardial dysfunction related to cardiotoxicity.

Acknowledgments

We are very appreciative of staff at the Imaging Center, Children's and Women's Hospital, University of South Alabama toward helping us acquire the MRI data. We thank Dr. Clive Woods for his help with proof reading and statistical analysis for this study. We greatly appreciate Dr. Fredrick Epstein's insight toward acquiring functional DENSE data in this specific patient subpopulation. We are also extremely appreciative of Dr. Michael Pasque for his clinical insight on the condition of cardiotoxicity.

Funding

This study was partly funded by NIH grant 1R21EB028063-01. This study was funded by University of South Alabama Award Number: A19-0028-001|Recipient: Julia Kar.

References

[1]. Cardinale D, Colombo A, Lamantia G, Colombo N, Civelli M, De Giacomi G, et al. Anthracycline-induced cardiomyopathy: clinical relevance and response to pharmacologic therapy. J Am Coll Cardiol 2010;55(3):213–20. [PubMed: 20117401]

[2]. Jurcut R, Wildiers H, Ganame J, D'Hooge J, Paridaens R, Voigt JU. Detection and monitoring of cardiotoxicity-what does modern cardiology offer? Support Care Cancer 2008;16(5):437–45. [PubMed: 18197426]

[3]. Khouri MG, Douglas PS, Mackey JR, Martin M, Scott JM, Scherrer-Crosbie M, et al. Cancer therapy-induced cardiac toxicity in early breast cancer: addressing the unresolved issues. Circulation 2012;126(23):2749–63. [PubMed: 23212997]

[4]. Stoodley P, Tanous D, Richards D, Meikle S, Clarke J, Hui R, et al. Trastuzumabinduced cardiotoxicity: the role of two-dimensional myocardial strain imaging in diagnosis and management. Echocardiography 2012;29(6):E137–40. [PubMed: 22381030]

[5]. Hare JL, Brown JK, Leano R, Jenkins C, Woodward N, Marwick TH. Use of myocardial deformation imaging to detect preclinical myocardial dysfunction before conventional measures in patients undergoing breast cancer treatment with trastuzumab. Am Heart J 2009;158(2):294–301. [PubMed: 19619708]

[6]. Jordan JH, Vasu S, Morgan TM, D'Agostino RB Jr., Melendez GC, Hamilton CA, et al. Anthracycline-associated T1 mapping characteristics are elevated independent of the presence of cardiovascular comorbidities in cancer survivors. Circ Cardiovasc Imaging 2016;9(8).

[7]. Hunt SA, Abraham WT, Chin MH, Feldman AM, Francis GS, Ganiats TG, et al. ACC/AHA 2005 Guideline Update for the Diagnosis and Management of Chronic Heart Failure in the Adult: a report of the American College of Cardiology/American Heart Association Task Force on Practice Guidelines (Writing Committee to Update the 2001 Guidelines for the Evaluation and Management of Heart Failure): developed in collaboration with the American College of Chest

Physicians and the International Society for Heart and Lung Transplantation: endorsed by the Heart Rhythm Society. Circulation 2005;112(12):e154–235. [PubMed: 16160202]

[8]. Slamon D, Eiermann W, Robert N, Pienkowski T, Martin M, Press M, et al. Adjuvant trastuzumab in HER2-positive breast cancer. N Engl J Med 2011;365(14):1273–83. [PubMed: 21991949]

[9]. Thavendiranathan P, Poulin F, Lim KD, Plana JC, Woo A, Marwick TH. Use of myocardial strain imaging by echocardiography for the early detection of cardiotoxicity in patients during and after cancer chemotherapy: a systematic review. J Am Coll Cardiol 2014;63(25 Pt A):2751–68. [PubMed: 24703918]

[10]. Sawaya H, Sebag IA, Plana JC, Januzzi JL, Ky B, Cohen V, et al. Early detection and prediction of cardiotoxicity in chemotherapy-treated patients. Am J Cardiol 2011;107(9):1375–80. [PubMed: 21371685]

[11]. Motoki H, Koyama J, Nakazawa H, Aizawa K, Kasai H, Izawa A, et al. Torsion analysis in the early detection of anthracycline-mediated cardiomyopathy. Eur Heart J Cardiovasc Imaging 2012;13(1):95–103. [PubMed: 21926409]

[12]. Mornos C, Petrescu L. Early detection of anthracycline-mediated cardiotoxicity: the value of considering both global longitudinal left ventricular strain and twist. Can J Physiol Pharmacol 2013;91(8):601–7. [PubMed: 23889668]

[13]. Jurcut R, Wildiers H, Ganame J, D'Hooge J, De Backer J, Denys H, et al. Strain rate imaging detects early cardiac effects of pegylated liposomal Doxorubicin as adjuvant therapy in elderly patients with breast cancer. Journal of the American Society of Echocardiography 2008;21(12):1283–9. [PubMed: 19041569]

[14]. Jones LW, Haykowsky MJ, Swartz JJ, Douglas PS, Mackey JR. Early breast cancer therapy and cardiovascular injury. J Am Coll Cardiol 2007;50(15):1435–41. [PubMed: 17919562]

[15]. Cardinale D, Colombo A, Bacchiani G, Tedeschi I, Meroni CA, Veglia F, et al. Early detection of anthracycline cardiotoxicity and improvement with heart failure therapy. Circulation 2015;131(22):1981–8. [PubMed: 25948538]

[16]. Sawaya H, Sebag IA, Plana JC, Januzzi JL, Ky B, Tan TC, et al. Assessment of echocardiography and biomarkers for the extended prediction of cardiotoxicity in patients treated with anthracyclines, taxanes, and trastuzumab. Circ Cardiovasc Imaging 2012;5(5):596–603. [PubMed: 22744937]

[17]. Stoodley PW, Richards DA, Hui R, Boyd A, Harnett PR, Meikle SR, et al. Two-dimensional myocardial strain imaging detects changes in left ventricular systolic function immediately after anthracycline chemotherapy. Eur J Echocardiogr 2011;12(12):945–52. [PubMed: 21965152]

[18]. Poterucha JT, Kutty S, Lindquist RK, Li L, Eidem BW. Changes in left ventricular longitudinal strain with anthracycline chemotherapy in adolescents precede subsequent decreased left ventricular ejection fraction. Journal of the American Society of Echocardiography 2012;25(7):733–40. [PubMed: 22578518]

[19]. Nakano S, Takahashi M, Kimura F, Senoo T, Saeki T, Ueda S, et al. Cardiac magnetic resonance imaging-based myocardial strain study for evaluation of cardiotoxicity in breast cancer patients treated with trastuzumab: a pilot study to evaluate the feasibility of the method. Cardiol J 2016;23(3):270–80. [PubMed: 27173679]

[20]. Grover S, Leong DP, Chakrabarty A, Joerg L, Kotasek D, Cheong K, et al. Left and right ventricular effects of anthracycline and trastuzumab chemotherapy: a prospective study using novel cardiac imaging and biochemical markers. Int J Cardiol 2013;168(6):5465–7. [PubMed: 24090744]

[21]. Seidman A, Hudis C, Pierri MK, Shak S, Paton V, Ashby M, et al. Cardiac dysfunction in the trastuzumab clinical trials experience. J Clin Oncol 2002;20(5):1215–21. [PubMed: 11870163]

[22]. Felker GM, Thompson RE, Hare JM, Hruban RH, Clemetson DE, Howard DL, et al. Underlying causes and long-term survival in patients with initially unexplained cardiomyopathy. N Engl J Med 2000;342(15):1077–84. [PubMed: 10760308]

[23]. Tan TC, Scherrer-Crosbie M. Cardiac complications of chemotherapy: role of imaging. Curr Treat Options Cardiovasc Med 2014;16(4):296. [PubMed: 24519487]

[25]. Sengupta PP, Tajik AJ, Chandrasekaran K, Khandheria BK. Twist mechanics of the left ventricle: principles and application. JACC Cardiovasc Imaging 2008;1(3):366–76. [PubMed: 19356451]

[26]. Russel IK, Gotte MJ, Bronzwaer JG, Knaapen P, Paulus WJ, van Rossum AC. Left ventricular torsion: an expanding role in the analysis of myocardial dysfunction. JACC Cardiovasc Imaging 2009;2(5):648–55. [PubMed: 19442954]

[27]. Notomi Y, Lysyansky P, Setser RM, Shiota T, Popovic ZB, Martin-Miklovic MG, et al. Measurement of ventricular torsion by two-dimensional ultrasound speckle tracking imaging. J Am Coll Cardiol 2005;45(12):2034–41. [PubMed: 15963406]

[28]. Kim D, Gilson WD, Kramer CM, Epstein FH. Myocardial tissue tracking with two-dimensional cine displacement-encoded MR imaging: development and initial evaluation. Radiology 2004;230(3):862–71. [PubMed: 14739307]

[29]. Spottiswoode BS, Zhong X, Hess AT, Kramer CM, Meintjes EM, Mayosi BM, et al. Tracking myocardial motion from cine DENSE images using spatiotemporal phase unwrapping and temporal fitting. IEEE Trans Med Imaging 2007;26(1):15–30. [PubMed: 17243581]

[30]. Aletras AH, Ding S, Balaban RS, Wen H. DENSE: displacement encoding with stimulated echoes in cardiac functional MRI. J Magn Reson 1999;137(1):247–52. [PubMed: 10053155]

[31]. Zhong X, Gibberman LB, Spottiswoode BS, Gilliam AD, Meyer CH, French BA, et al. Comprehensive cardiovascular magnetic resonance of myocardial mechanics in mice using three-dimensional cine DENSE. J Cardiovasc Magn Reson 2011;13:83. [PubMed: 22208954]

[32]. Zhong X, Spottiswoode BS, Meyer CH, Kramer CM, Epstein FH. Imaging three-dimensional myocardial mechanics using navigator-gated volumetric spiral cine DENSE MRI. Magnetic Resonance in Medicine 2010;64(4):1089–97. [PubMed: 20574967]

[33]. Kar J, Zhong X, Cohen MV, Cornejo DA, Yates-Judice A, Rel E, et al. Introduction to a mechanism for automated myocardium boundary detection with displacement encoding with stimulated echoes (DENSE). Br J Radiol 2018;91(1087):20170841. [PubMed: 29565646]

[34]. McGowan JV, Chung R, Maulik A, Piotrowska I, Walker JM, Yellon DM. Anthracycline chemotherapy and cardiotoxicity. Cardiovasc Drugs Ther 2017;31(1):63–75. [PubMed: 28185035]

[35]. Carver JR, Shapiro CL, Ng A, Jacobs L, Schwartz C, Virgo KS, et al. American Society of Clinical Oncology clinical evidence review on the ongoing care of adult cancer survivors: cardiac and pulmonary late effects. J Clin Oncol 2007;25(25):3991–4008. [PubMed: 17577017]

[36]. Kar J, Knutsen AK, Cupps BP, Zhong X, Pasque MK. Three-dimensional regional strain computation method with displacement encoding with stimulated echoes (DENSE) in non-ischemic, non-valvular dilated cardiomyopathy patients and healthy subjects validated by tagged MRI. Journal of Magnetic Resonance Imaging 2015;41(2):386–96. [PubMed: 24753028]

[37]. Zhong X, Helm PA, Epstein FH. Balanced multipoint displacement encoding for DENSE MRI. Magnetic Resonance in Medicine 2009;61(4):981–8. [PubMed: 19189288]

[38]. Liao PS, CT S, Chung PC. A fast algorithm for multilevel thresholding. J Inf Sci Eng 2001;17(5):713–27.

[39]. Otsu N A threshold selection method from gray-level histograms. IEEE Trans Syst Man Cybern 1979;9(1):62–6.

[40]. Kar J, Knutsen AK, Cupps BP, Pasque MK. A validation of two-dimensional in vivo regional strain computed from displacement encoding with stimulated echoes (DENSE), in reference to tagged magnetic resonance imaging and studies in repeatability. Ann Biomed Eng 2014;42(3):541–54. [PubMed: 24150239]

[41]. Spottiswoode BS, Zhong X, Lorenz CH, Mayosi BM, Meintjes EM, Epstein FH. Motion-guided segmentation for cine DENSE MRI. Med Image Anal 2009;13(1):105–15. [PubMed: 18706851]

[42]. Liu GR. Meshfree methods: Moving beyond the finite element method. 2 ed Raton Boca: CRC Press; 2009.

[43]. Wang JG, Liu GR. A point interpolation meshless method based on radial basis functions. Int J Numer Methods Eng 2002;54:1623–48.

[44]. Wang JG, Liu GR. On the optimal shape parameters of radial basis functions used for 2-D meshlesss methods. Comput Methods Appl Mech Eng 2002;191(23–24):2611–30.

[45]. Andre F, Steen H, Matheis P, Westkott M, Breuninger K, Sander Y, et al. Age- and gender-related normal left ventricular deformation assessed by cardiovascular magnetic resonance feature tracking. J Cardiovasc Magn Reson 2015;17:25. [PubMed: 25890093]

[46]. Yoneyama K, Gjesdal O, Choi EY, Wu CO, Hundley WG, Gomes AS, et al. Age, sex, and hypertension-related remodeling influences left ventricular torsion assessed by tagged cardiac magnetic resonance in asymptomatic individuals: the multi-ethnic study of atherosclerosis. Circulation 2012;126(21):2481–90. [PubMed: 23147172]

[47]. Cain PA, Ahl R, Hedstrom E, Ugander M, Allansdotter-Johnsson A, Friberg P, et al. Age and gender specific normal values of left ventricular mass, volume and function for gradient echo magnetic resonance imaging: a cross sectional study. BMC Med Imaging 2009;9:2. [PubMed: 19159437]

[48]. Pinder MC, Duan Z, Goodwin JS, Hortobagyi GN, Giordano SH. Congestive heart failure in older women treated with adjuvant anthracycline chemotherapy for breast cancer. J Clin Oncol 2007;25(25):3808–15. [PubMed: 17664460]

[49]. Kar J, Baldwin BM, Cohen MK, Joseph S, Chowdry A, Figarola MS, et al. A case-study in MRI-based automated detection of left-ventricular cardiotoxicity in a breast cancer patient afterchemotherapy treatment. Soc Cardiovasc Magn Reson. SCMR 2019 https://www.cloudcmr.com/3357-1973-2158-0172.

[50]. Kar J, Cupps B, Zhong X, Koerner D, Kulshrestha K, Neudecker S, et al. Preliminary investigation of multiparametric strain Z-score (MPZS) computation using displacement encoding with simulated echoes (DENSE) and radial point interpretation method (RPIM). Journal of magnetic resonance imaging: JMRI 2016;44(4):993–1002. [PubMed: 27038246]

[51]. Kuznetsova T, Thijs L, Knez J, Cauwenberghs N, Petit T, Gu YM, et al. Longitudinal changes in left ventricular diastolic function in a general population. Circ Cardiovasc Imaging 2015;8(4).

[52]. Gotte MJ, Germans T, Russel IK, Zwanenburg JJ, Marcus JT, van Rossum AC, et al. Myocardial strain and torsion quantified by cardiovascular magnetic resonance tissue tagging: studies in normal and impaired left ventricular function. J Am Coll Cardiol 2006;48(10):2002–11. [PubMed: 17112990]

[53]. Hudsmith LE, Petersen SE, Francis JM, Robson MD, Neubauer S. Normal human left and right ventricular and left atrial dimensions using steady state free precession magnetic resonance imaging. J Cardiovasc Magn Reson 2005;7(5):775–82. [PubMed: 16353438]

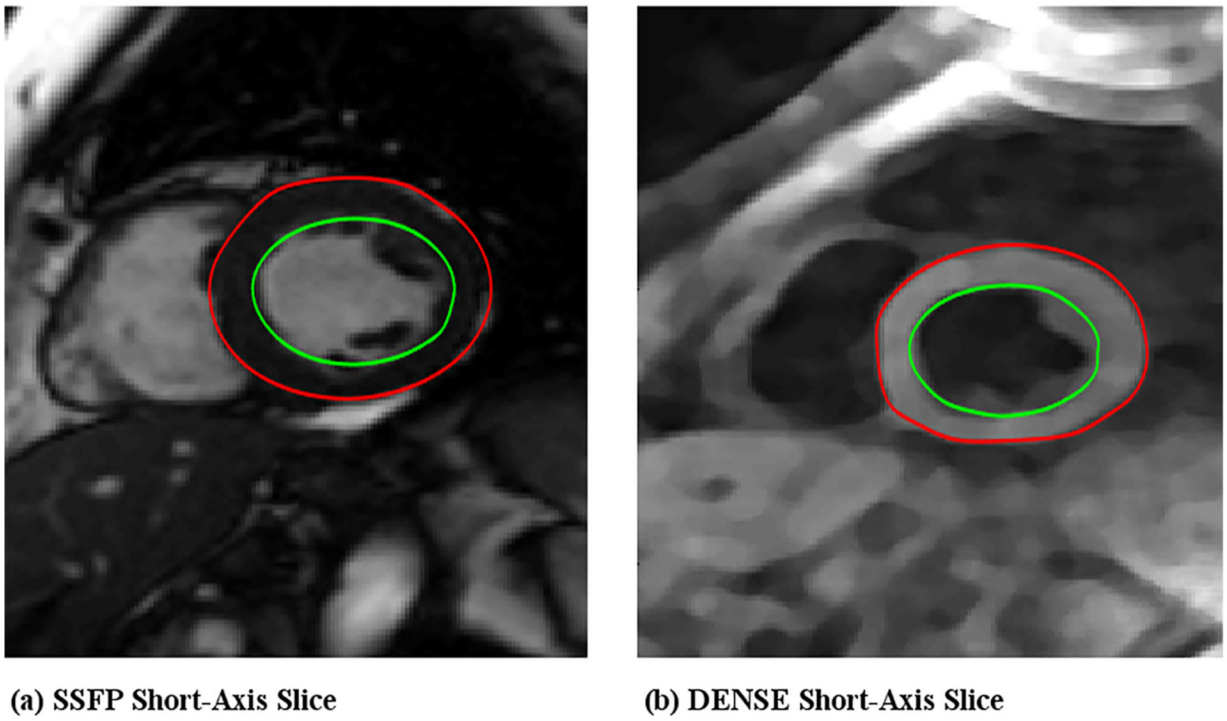

Fig. 1.

Left-ventricular ejection fractions (LVEF) were computed from myocardial boundaries detected using the automated strain analysis algorithm in (a) SSFP and (b) DENSE short-axis images of patients and compared to validate the chamber quantification algorithm.

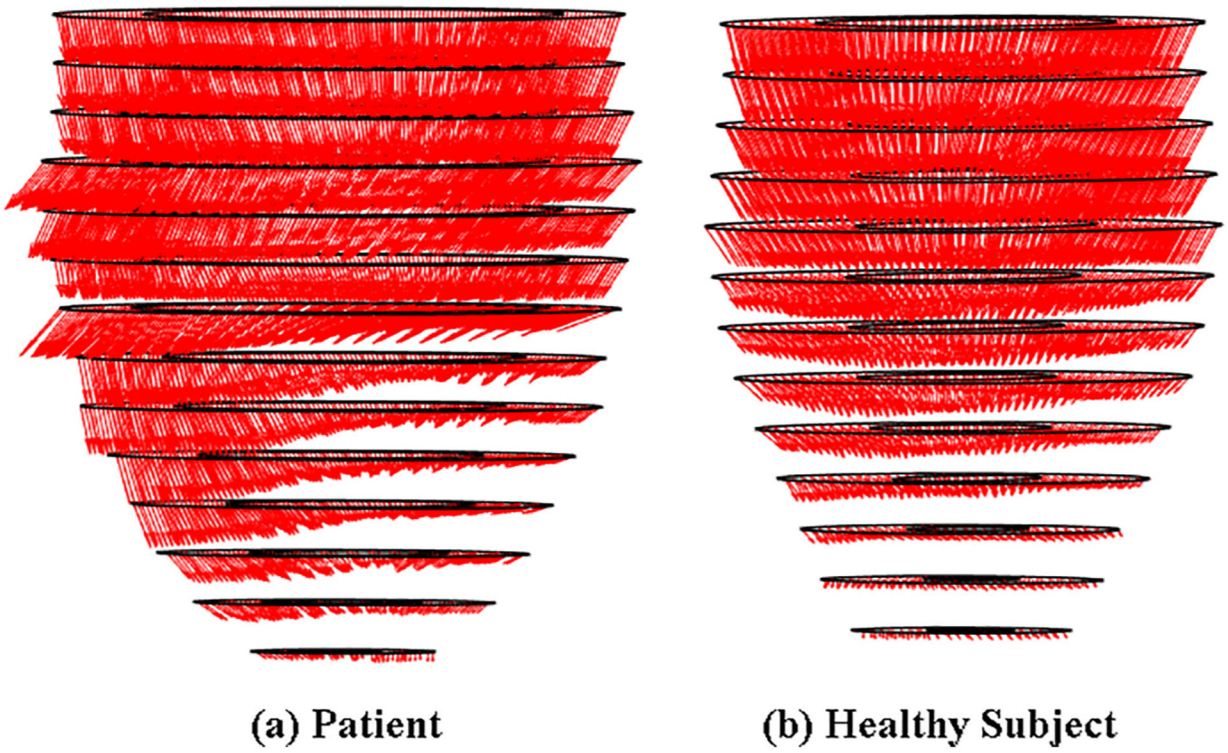

Fig. 2.

Phase-unwrapping based 3D displacement vectors computed in the full LV of (a) a patient and (b) a healthy subject.

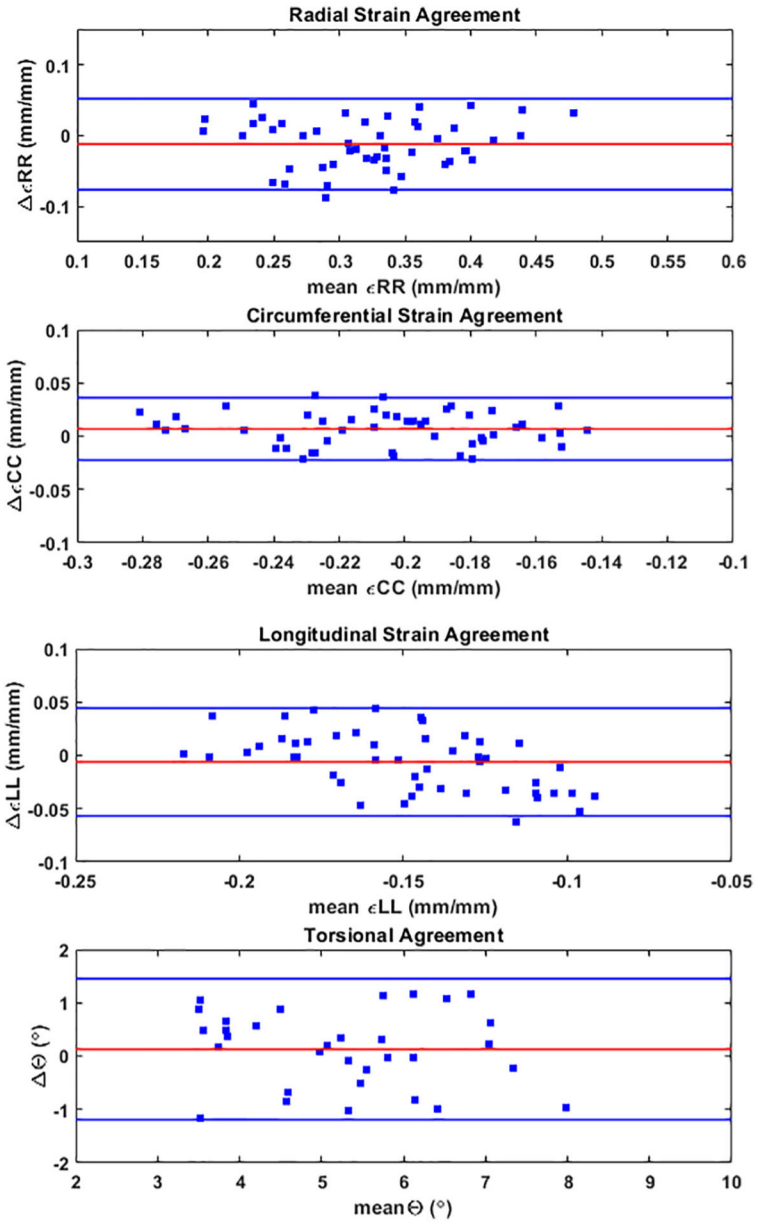

Fig. 3.

Interobserver agreements measured with Bland-Altman analysis for radial, circumferential and longitudinal strains and torsion in the patient subpopulation, which were computed with the 3D automated strain analysis algorithm. The strain parameters were calculated in three segments (apical, mid-ventricular and basal) for each of the 16 patients and torsion in the apical and mid-ventricular segments (relative to base) in the 16 patients by each of two observers.

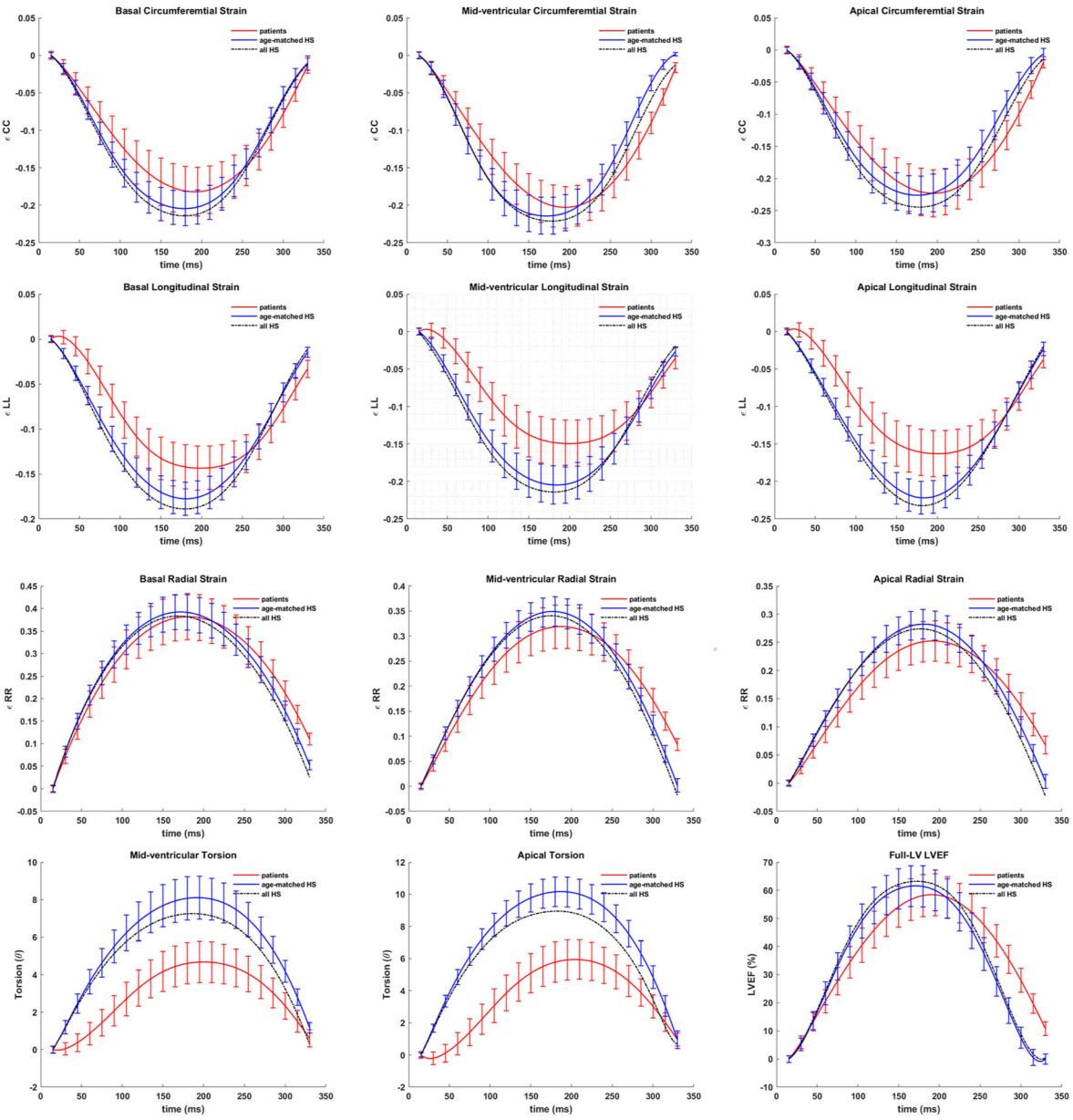

Fig. 4.

Trajectories of basal, mid-ventricular and apical circumferential, longitudinal and radial strains, mid-ventricular and apical torsion (°) and LVEF (%) in the patient population and age-matched healthy subjects and in the entire healthy subpopulation (broken lines). Abbreviations: HS: healthy subjects.

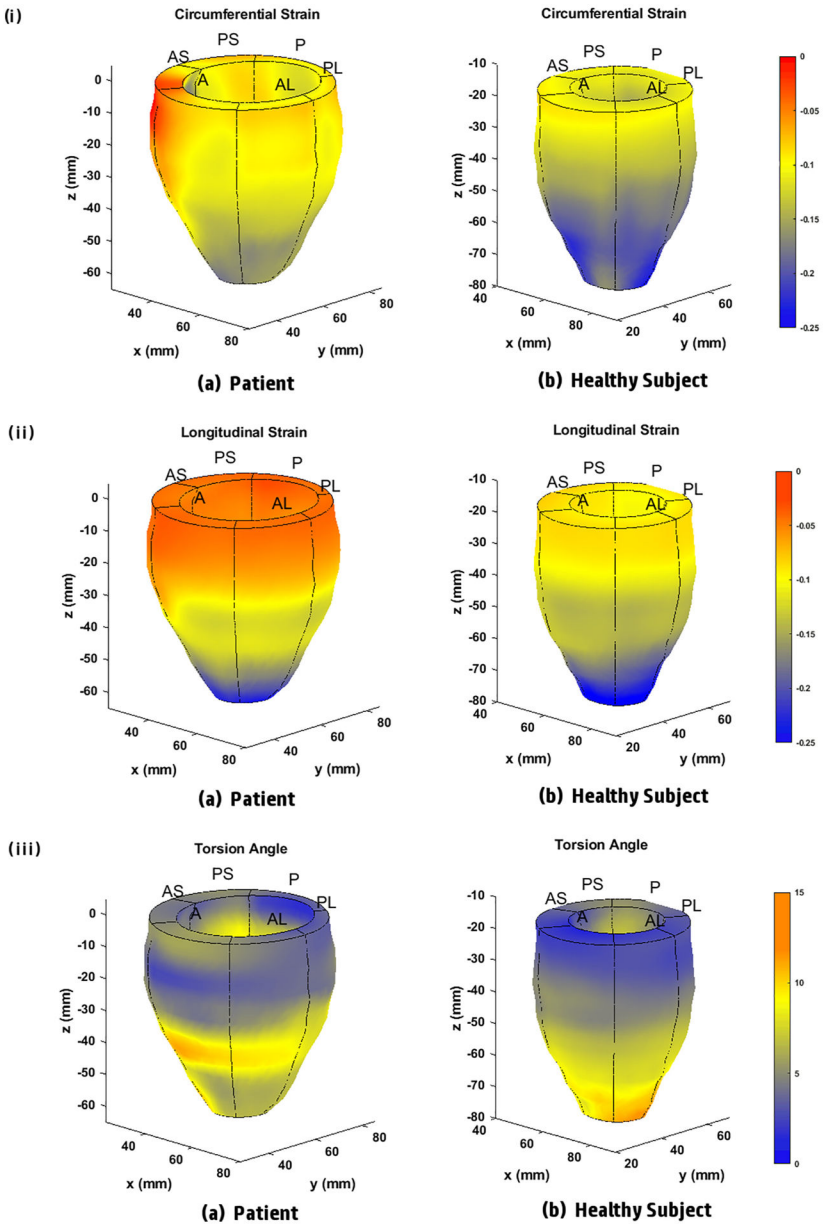

Fig. 5.

Three-dimensional (i) circumferential strain (ii) longitudinal strain and (iii) torsion maps generated with the automated strain analysis algorithm in the full LV of (a) a patient and (b) a healthy subject.

Table 1

Demographics, comorbidities and chamber quantifications in patient and healthy subjects.

Parameter	Patients	Age-matched HS	p-Value
Demographics			
Age (years)	54.9 ± 8.9	48.5 ± 7.2	0.05
SBP (mmHg)	126.9 ± 14.5	123 ± 8.4	0.50
DBP (mmHg)	73.8 ± 11.3	67.9 ± 6.6	0.10
HR (bpm)	76.1 ± 11	69.2 ± 7.6	0.06
Body Mass (kg)	77.2 ± 14.1	76.2 ± 13.5	0.80
BMI (kg/cm^2)	1.9 ± 0.2	1.9 ± 0.2	0.90
BSA (m^2)	28.8 ± 6.4	28.5 ± 4.8	0.90
Comorbidities			
Hypertension	4	0	0.03 *
Hypercholesterolemia	3	0	0.07
Diabetes mellitus	2	0	0.20
Chemotherapy dose			
Doxorubicin 240 mg/m^2	11	0	0.00 ++
Trastuzumab 8 mg/kg loading + 6 mg/kg	5	0	0.01 *
Radiotherapy	6	0	0.00 ++
Chamber quantifications			
Diameter basal (D) (cm)	5.2 ± 0.5	4.5 ± 0.5	0.00 ++
Diameter mid (D) (cm)	4.0 ± 0.4	3.7 ± 0.4	0.10
Diameter apical (D) (cm)	3.1 ± 0.4	2.9 ± 0.3	0.20
Diameter basal (S) (cm)	3.4 ± 0.4	2.9 ± 0.3	0.00 ++
Diameter mid (S) (cm)	2.5 ± 0.3	2.4 ± 0.3	0.50
Diameter apical (S) (cm)	1.8 ± 0.3	1.6 ± 0.2	0.10
EDV full LV (cm^3)	112.6 ± 15.8	108.5 ± 14.5	0.60
ESV full LV (cm^3)	46.8 ± 10.3	41.7 ± 8.4	0.30
SV full LV (cm^3)	66.0 ± 12.7	66.7 ± 11.9	0.90
EF full LV (%)	58 ± 7	62 ± 5	0.40
Full LV mass (gm)	127.6 ± 8.3	134.5 ± 9.5	0.30

Abbreviations: DBP: diastolic blood pressure (BP), SBP: systolic BP, HR: heart rate, BMI: body mass index, BSA: body surface area HS: healthy subjects, D: diastolic, S: systolic, EDV: end diastolic volume, ESV: end systolic volume, SV: stroke volume, EF: ejection fraction.

*Significant differences between patients and healthy subjects.

++$p < 0.01$.

Table 2

Strain parameters in patients and healthy subjects.

Parameter	Patients	Age-matched HS	p-Value
E_{cc} basal	−0.18 ± 0.03	− 0.20 ± 0.02	0.20
E_{cc} mid	− 0.20 ± 0.03	− 0.21 ± 0.03	0.50
E_{cc} apical	− 0.22 ± 0.03	− 0.23 ± 0.03	0.90
E_{cc} global	− 0.20 ± 0.03	− 0.21 ± 0.03	0.50
E_{ll} basal	− 0.14 ± 0.02	− 0.18 ± 0.02	0.01*
E_{ll} mid	− 0.15 ± 0.03	− 0.20 ± 0.02	0.00**
E_{ll} apical	− 0.16 ± 0.03	− 0.22 ± 0.02	0.00**
E_{ll} global	− 0.15 ± 0.02	− 0.20 ± 0.02	0.00**
E_{rr} basal	0.38 ± 0.05	0.39 ± 0.04	0.60
E_{rr} mid	0.32 ± 0.04	0.35 ± 0.03	0.10
E_{rr} apical	0.25 ± 0.04	0.28 ± 0.03	0.10
E_{rr} global	0.32 ± 0.04	0.34 ± 0.03	0.20
Rotation bas (°)	− 1.60 ± 1.20	− 4.80 ± 3.10	0.00**
Rotation mid (°)	5.40 ± 1.50	8.70 ± 2.20	0.01*
Rotation apex (°)	8.60 ± 2.20	12.20 ± 2.80	0.01*
Torsion bas (°)	0.00 ± 0.00	0.00 ± 0.00	–
Torsion mid (°)	4.70 ± 1.00	8.10 ± 1.10	0.00**
Torsion apical (°)	5.90 ± 1.20	10.20 ± 0.90	0.00**

Abbreviations: HS: healthy subjects, rr: radial, cc: circumferential, ll: longitudinal.

*Significant differences between patients and healthy subjects.

**$p < 0.001$.